Chapter

Phase-Shift Transmission Line Method for Permittivity Measurement and Its Potential in Sensor Applications

Vasa Radonic, Norbert Cselyuszka, Vesna Crnojevic-Bengin and Goran Kitic

Abstract

This chapter offers a detailed insight into a dielectric characterization of the materials based on the phase-shift measurements of the transmission signal. The chapter will provide in-depth theoretical background of the phase-shift transmission line measurement in the microstrip architecture and determination of dielectric permittivity of design under test for several measurement configurations. Potential of the phase-shift method will be demonstrated through applications in the characterization of an unknown dielectric constant in multilayered structure, realization of the soil moisture sensor, and sensor for determination of the dielectric constant of a fluid in microfluidic channel. Moreover, specific techniques for increasing the phase shift based on the electromagnetic bandgap structure, the aperture in the ground plane and the left-handed effect will be presented. In the end, the realization of simple in-field detection device for determination of permittivity based on the phase-shift measurement will be demonstrated.

Keywords: phase-shift method, transmission line, microstrip, permittivity, sensors

1. Introduction

The measurement of dielectric properties of the materials found application in different fields, such as material science, absorber development, biomedical research, tissue engineering, wood industry, food quality control, etc. [1–5]. A number of methods have been developed over a time for characterization of the dielectric properties of the materials such as time domain method [6, 7], capacitive method [3, 8], transmission line (TL) methods [3, 9, 10], resonant method [3, 9], etc. The selection of the appropriate method depends on the measured frequency range, expected values of permittivity, measurement accuracy, form of material (solid, powder, and liquid), sample shape and size, temperature, etc. [8, 11]. Moreover, depending on some important aspects, the measurement methods can be divided into contact or noncontact methods (depends on whether the sample is

touched or not), destructive or nondestructive (depends on whether sample can be destroyed or not), narrowband and wideband (depends on frequency range), etc. Since each method has its own advantages and limitations, the selection of the appropriate one depends on a particular application, required accuracy, sample, and other factors. There are a number of commercially available holders, kits, and probes that operate on different principles and allow measurement of the dielectric constant of the material in different forms on different temperatures and frequency ranges [8, 11]. However, the most of them are designed to be connected with expensive instruments such as network analyzers, LCR meters, or impedance analyzers.

One of the commonly used methods suitable for the material characterization in a wide frequency range, from around 10 MHz to 75 GHz, is the TL method. The TL method includes both measurements of the reflection and/or transmission characteristic [3–10]. This method can be used for characterization of permittivity as well as permeability of hard solid materials with medium losses. High-loss materials can be also characterized using this method, if the sample is kept relatively thin. The TL holders are usually made of a coaxial, a waveguide, or a microstrip line section. However, the specific design of the holder or specific multilayered configurations can be used for characterization of powders, liquid, or gases. Usually, the method requires initial sample preparation to fit into the section of the TL, typically the waveguide or the coaxial line. For accurate permittivity measurement, the sample has to be exposed to the maximal electric field, and therefore the position of the sample is very important. A typical measurement configuration of this method consists of the TL section with a sample placed inside, a vector network analyzer (VNA) used to measure the two ports complex scattering parameters (S-parameters), and a software that converts the measured S-parameters to the complex permittivity or permeability. In addition, the TL method requires initial calibration with various terminations before the measurement.

The measurement of the phase shift of the transmitted signal represents relatively fast and simple method for determination of the dielectric properties of the material. It is characterized by fast time response, and in comparison with other methods, it is less sensitive to the noise [10, 12]. Furthermore, this method allows characterization at a single frequency which simplifies the development of a supporting electronic, allows easy integration with sensor element, and allows realization of low-cost in-field sensing devices. Therefore, it found application in the realization of different types of sensors such as soil moisture sensors [13], microfluidic sensor for detention fluid mixture concentration [14], etc.

In this chapter, the phase-shift method will be explained on the example of a microstrip line configuration, and the permittivity of the materials will be determined by measuring the phase shift of the transmitted signal. Theoretical background of the phase-shift method and mathematical equations for determination of real and imaginary part of complex permittivity based on the phase of the transmitted signal will be presented in Section 2. The unknown permittivity of material will be determined for several measurement configurations in Section 3. Potential of the phase-shift method will be demonstrated through several applications in the characterization of an unknown dielectric constant in multilayered structure, a soil moisture sensor, and sensor for determination of fluid properties in microfluidic channel. Advance techniques for increasing the sensitivity of the phase-shift measurement will be presented in Section 4, while the simple in-field detection device for determination of the permittivity based on the phase measurement will be presented in Section 5. The conclusions are given in Section 6.

2. Phase-shift method

2.1 Determination of real part of the dielectric constant

Phase-shift method is based on the measurement of the phase shift of a sinusoidal signal that propagates along a transmission line.

Phase shift $\Delta\varphi$ is defined by velocity and frequency of the propagating signal as well as physical properties of the transmission line:

$$\Delta\varphi = \frac{\omega L_{TL}}{v_p}, \tag{1}$$

where ω is the angular frequency, v_p is the phase velocity, and L_{TL} is the length of transmission line.

In order to determine a phase velocity of electromagnetic wave, we will start with the expression for imaginary part of the complex propagation constant for lossy medium [15]:

$$\beta = \frac{\omega\sqrt{\mu\varepsilon}}{\sqrt{2}}\sqrt{1+\sqrt{1+\frac{\sigma^2}{\omega^2\varepsilon^2}}}, \tag{2}$$

where μ, ε, and σ are the real parts of the permeability, permittivity, and electrical conductivity of the medium through which the signal is propagating, respectively. If the imaginary part of the complex propagation constant is known, the phase velocity can be determined as

$$v_p = \frac{\omega}{\beta} = \frac{\sqrt{2}}{\sqrt{\mu\varepsilon}}\frac{1}{\sqrt{1+\sqrt{1+\frac{\sigma^2}{\omega^2\varepsilon^2}}}}. \tag{3}$$

Based on Eq. (3), it can be seen that phase velocity is dominantly influenced by permittivity, permeability and signal frequency, and then electrical conductivity.

The main advantage of the phase-shift method lies on the fact that on the frequencies high enough, the influence of conductivity can be neglected:

$$\frac{\sigma^2}{\omega^2\,\varepsilon^2} \ll 1; \tag{4}$$

therefore, expression for velocity on high frequencies can be reduced to

$$v_p = \frac{1}{\sqrt{\mu\varepsilon}}, \tag{5}$$

where phase velocity is determined by permeability and permittivity only. This is especially important for soil moisture sensor which will be discussed later since most of the materials in the soil are diamagnetic or paramagnetic. If we assume that electromagnetic wave propagates through a nonmagnetic medium, that is, the magnetic permeability is equal to $\mu_0 = 4\pi \bullet 10^{-7}$ H/m, the phase velocity and the phase shift are dependent on dielectric permittivity only:

$$\Delta\varphi = \omega L_{TL}\sqrt{\mu_0\varepsilon} = \omega L_{TL}\sqrt{\mu_0\varepsilon_0\varepsilon_r} = \frac{\omega L_{TL}}{c_0}\sqrt{\varepsilon_r}, \tag{6}$$

where c_0 is the speed of the light in the vacuum and ε_r is a relative dielectric constant of the medium.

Unlike the coaxial line or the waveguide, the microstrip structure is particularly interesting for a simple and low-cost fabrication of compact sensors based on dielectric permittivity change which can be easily integrated with supporting electronics. In this way, standard printed circuit board technology used for microstrip manufacturing offers fabrication of a complete solution of the sensor in a single substrate. Therefore, the concept of the phase-shift measurement will be explained on the example of microstrip line. In the microstrip, the influence of the change in permittivity is reflected in effective permittivity which is determined by permittivity of a medium above the microstrip line and permittivity of the dielectric substrate, **Figure 1**.

Effective permittivity of the microstrip line shown in **Figure 1** can be expressed as

$$\varepsilon_{eff} = \frac{\varepsilon_s + \varepsilon_m}{2} + \frac{\varepsilon_s - \varepsilon_m}{2} \frac{1}{\sqrt{1 + 12\frac{h}{w}}}, \tag{7}$$

where ε_r and ε_m are the permittivity of dielectric substrate and the medium above the line, respectively, h is the height of the substrate, and w is the width of the microstrip line [16].

It can be seen that a variation in the permittivity of the medium causes a variation in effective permittivity that results in the change of the phase velocity. The change in the phase velocity changes the phase shift of the signal. It is evident that phase shift is determined by the value of the permittivity of the medium above the microstrip line. Therefore, the real part of dielectric constant of unknown medium can be detected with simple measurement of the phase shift of the transmitted signal.

The range of the phase shift $\Delta\Phi$, is determined by the upper and lower values of the measured permittivity:

$$\Delta\Phi = \Delta\varphi_{max} - \Delta\varphi_{min} = \omega L_{TL}\sqrt{\mu_0\varepsilon_0}\left(\sqrt{\varepsilon_{eff\,max}} - \sqrt{\varepsilon_{eff\,min}}\right). \tag{8}$$

This parameter needs to be adjusted to the supporting electronics that measure the phase shift. From Eq. (8) it can be seen that with appropriate choice of the operating frequency and the proper optimization of the geometrical parameters (mostly the length of the transmission line), the range of the phase shift can be optimized to the maximal measurable value.

As stated above, the phase shift depends on the properties of the transmission line. Since the microstrip line can be characterized by inductance per unit length, L',

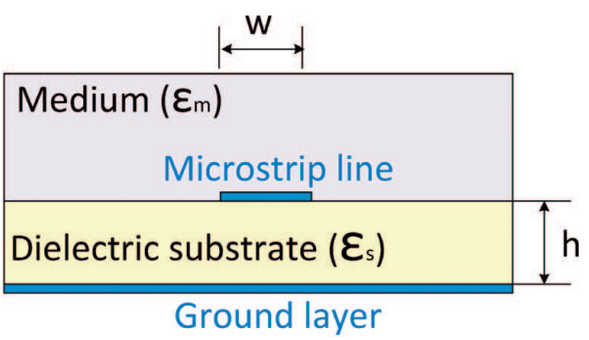

Figure 1.
Configuration of the microstrip line.

and capacitance per unit length, C', on high frequencies, the phase velocity of the signal that propagates along microstrip can be defined as [17]

$$v_p = \frac{1}{L'C'}. \tag{9}$$

Combining Eqs. (1) and (9), phase shift of the signal propagating along microstrip line with length L_{TL} can be expressed as

$$\Delta\varphi = \omega \mathrm{L_{TL}} \sqrt{L'C'} = \omega\sqrt{LC}, \tag{10}$$

while the phase-shift range is

$$\Delta\Phi = \Delta\varphi_{max} - \Delta\varphi_{min} = \omega\left(\sqrt{L_{max}C_{max}} - \sqrt{L_{min}C_{min}}\right). \tag{11}$$

The capacitance can be written in the form of the vacuum capacitance C_0, which represents the capacitance of the microstrip line when both substrate and medium relative permittivities are equal to 1, and effective permittivity

. $$C = C_0\varepsilon_{eff}. \tag{12}$$

In addition, if we assume that the electromagnetic wave propagates through a nonmagnetic medium, the inductivity of the transmission line does not depend on the sample under test ($L_{max} = L_{min} = \ L$). Therefore, the expression for the phase-shift range can be reduced to

$$\Delta\Phi = \omega\sqrt{LC_0}\left(\sqrt{\varepsilon_{eff\,max}} - \sqrt{\varepsilon_{eff\,min}}\right). \tag{13}$$

Based on Eq. (13), it can be concluded that the phase-shift range can be increased by performing the measurements on higher frequencies or by increasing the total microstrip line inductance or capacitance. Therefore, the phase-shift range can be optimized to the capabilities of the supporting electronics for measurement of the phase shift.

To validate the proposed method for the characterization of the material properties in wider frequency range, we compare the results of the dielectric constant calculated using proposed method with a predetermined value of dielectric constant, **Figure 2**. For the comparison, the microstrip transmission line was used where the unknown medium was placed above the microstrip line and dielectric substrate, as shown in **Figure 1**. The calculated dielectric constant was extracted from the phase shift of the transited signal using described procedure. The proposed result reveals that the phase-shift detection method provides high accuracy with the relative errors lower than 0.5% for the real parts of the dielectric constant in the measured frequency range.

2.2 Determination of the imaginary part of the dielectric constant

From the previous analysis, we demonstrate how the real part of the complex permittivity can be determined from the phase shift of the transmitted signal. However, the imaginary part of the complex permittivity cannot be directly calculated from the phase shift. It can be estimated using Kramers-Kronig (K-K) relation [18–22].

The real and imaginary part of the complex dielectric constant is correlated with K-K relation [18–20]. This relation is a direct consequence of the principle of

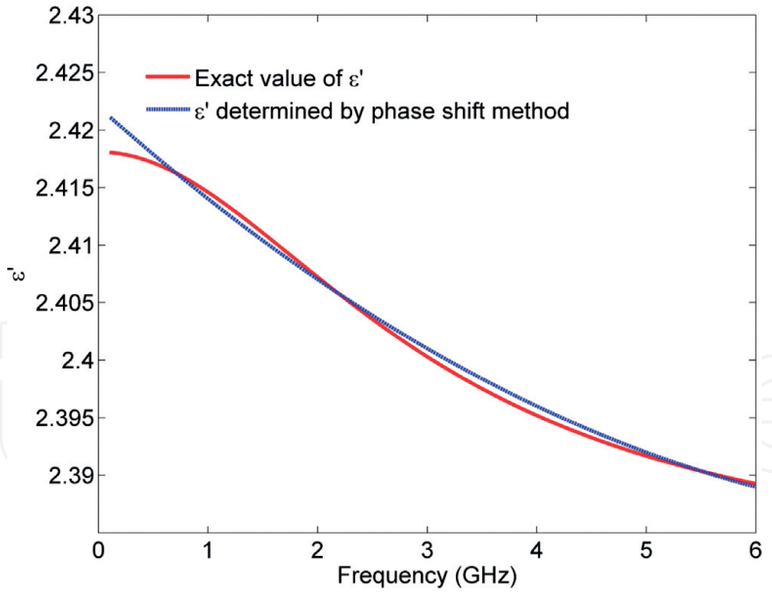

Figure 2.
Real part of the dielectric constant calculated using the phase-shift method compared with the predetermined value.

causality [21]. K-K relation describes a fundamental correlation between the real and imaginary part of the complex dielectric constant and allows us to retrieve imaginary part of the dielectric constant from the measured real part or vice versa.

The imaginary part of the complex dielectric constant can be calculated as

$$\varepsilon''(\omega) = -\frac{2\omega}{\pi}\wp\int_0^\infty \frac{\varepsilon'(\Omega)-1}{\Omega^2-\omega^2}d\Omega, \tag{14}$$

where ω is the angular frequency, ε' is the frequency-dependent real part of the dielectric constant, and $\wp$ is the Cauchy principal value [22].

The imaginary part of the complex dielectric constants retrieved using K-K relation from the real part of the dielectric constant (**Figure 2**) measured by phase-shift method is shown in **Figure 3**. The calculated imaginary part shows a good

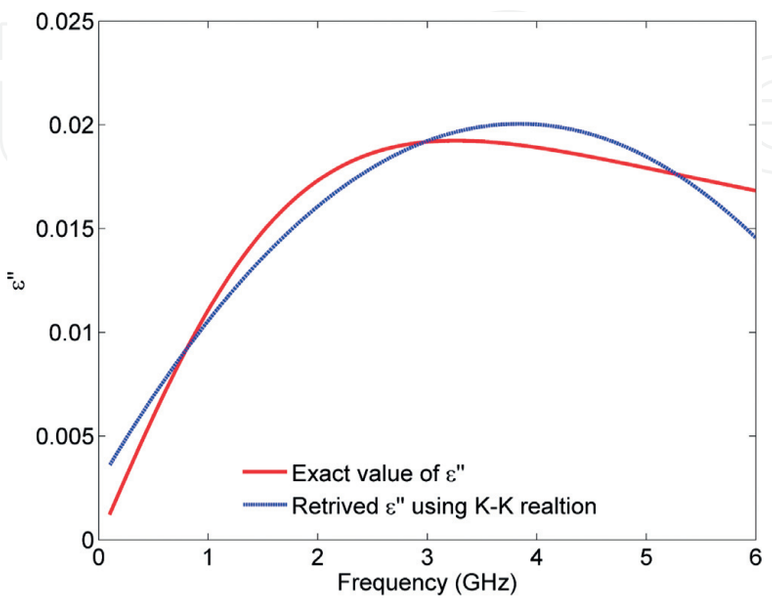

Figure 3.
Imaginary part of the complex dielectric constant retrieved by K-K relation from real part of the dielectric constant measured by phase-shift method.

agreement with the predetermined value of imaginary parts. However, the relative error is about 9% since the accuracy of Eq. (14) depends on the measured frequency range. It can be noted that the range from 0 to ∞ in the integral in Eq. (14) is not achievable in practice. Therefore, the limited range of frequencies affects the accuracy of the results and causes the error that can be observed in **Figure 3**.

3. Multilayered substrate configurations

In a previous section, we presented how the real and imaginary parts of the dielectric constant of the conventional microstrip configuration can be determined using the phase-shift method based on the phase of the transmitted signal. The same method can be applied for nonhomogeneous substrate such as multilayered or heterogeneous substrate. In this section we will analyze different microstrip multilayered substrate configurations interesting for the realization of different sensor topologies. The phase-shift method will be used for the calculation of the effective dielectric constant and determination of the real part of dielectric constant of individual layers. Similarly, the imaginary part of the complex permittivity can be determined from real part using procedure described in Section 2.2.

If we assume that the microstrip transmission line is realized on a multilayered substrate consisting of N layers with different dielectric constants, the effective dielectric constant, ε_s, of the multilayer substrate with N layers can be calculated using [14, 23]

$$\varepsilon_s = \frac{\sum_{i=1}^{N} |d_i|}{\sum_{i=1}^{N} \left| \frac{d_i}{\varepsilon_i} \right|}, \tag{15}$$

where N is the number of the layers, ε_i is the dielectric constant of the i-th layer, and d_i is a coefficient which can be calculated using the following equation:

$$d_i = \frac{K(k_i)}{K'(k_i)} - \frac{K(k_{i-1})}{K'(k_{i-1})} \cdots - \frac{K(k_1)}{K'(k_1)}, \tag{16}$$

where K and $K' = K(k_i)$ are the complete elliptical integrals of the first kind [24] and k_i is

$$k_i = \frac{1}{\cosh\left(\frac{\pi w}{4\sum_{i=1}^{N} h_i}\right)}, \tag{17}$$

where w is the width of the microstrip line and h_i is the thickness of the i-th layer. If all geometrical parameters are known as well as the dielectric constants of all layers except of one arbitrary layer, this unknown dielectric constant can be determined based on effective dielectric constant of the multilayered substrate. Previously, the effective dielectric constant has to be determined from the phase shift of the transmitted signal.

If the parameters of several layers are unknown, the unknown values of the dielectric constants can be found by solving system of equations. This procedure requires several measurements with different sets of geometrical parameters, typically the length of the microstrip line. In that case, the number of the essential measurements required for the determination of all parameter depends on the number of the unknown materials.

Beside conventional microstrip line, next three examples present typical microstrip configurations commonly used in the sensor design. Therefore, the determination of the dielectric constant will be explained on bilayered, tri-layered, and the embedded substrate configurations. In the following section, the practical applications of the analyzed configurations will be demonstrated.

The simplest case is a microstrip line realized on a bilayer substrate, shown in **Figure 4**, when the property of one layer is known (ε_{r1}) and the other one is unknown (ε_{r2}). This presents a typical configuration of the microstrip sensor with thin sensitive film deposited on the dielectric substrate.

The effective dielectric constant of the substrate combination bellow microstrip line (ε_s) can be obtained using procedure explained in Section 2, while the unknown dielectric constant in the bilayered configuration can be expressed as

$$\varepsilon_{r2} = d_2\left[\pm\left(\frac{|d_1|+|d_2|}{\varepsilon_s} - \frac{|d_1|}{|\varepsilon_{r1}|}\right)\right]^{-1}, \tag{18}$$

where coefficients d_i can be obtained using Eq. (16).

The example of the calculated unknown dielectric constant in the bilayered configuration is shown in **Figure 5**. The preset values for the dielectric constants were set to constant value of ε_{r1} = 3.6 and ε_{r2} = 2.4, while the geometrical parameters of the microstrip line were set to h_1 = 0.1 mm, h_2 = 0.2 mm, and w = 1.5 mm, and the length of the microstrip line was set to L = 10 mm. It can be seen that the

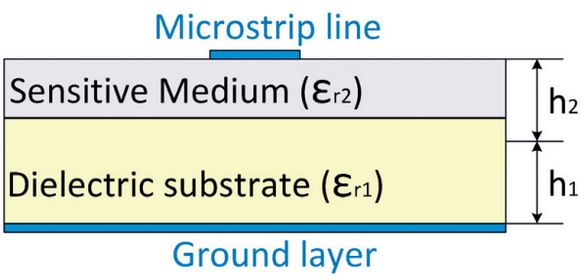

Figure 4.
Microstrip line on bilayered substrate.

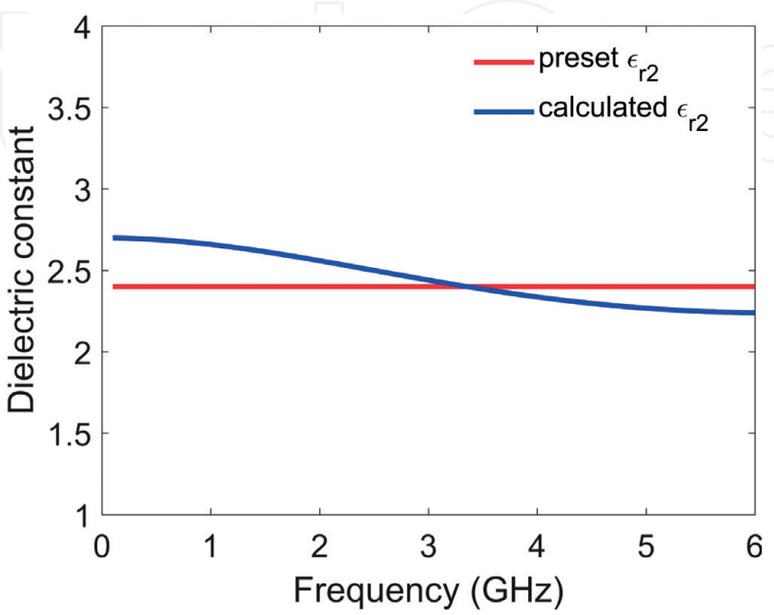

Figure 5.
Calculated unknown dielectric constant in the bilayered substrate combination.

calculated dielectric constant is in a good agreement with the preset value in the calculated frequency range.

Another example presents tri-layered substrate where middle layer is the one with an unknown dielectric constant, **Figure 6**. The bottom and top layers have the same known dielectric contestants, while the middle one is with an unknown material and with known geometrical parameters. This geometrical configuration is typical for the realization of the sensor for the characterization of a fluid or gasses in which the reservoir is placed between two dielectrics bellow microstrip line [25, 26].

Using above-described procedure, the effective dielectric constant of the tri-layer substrate (ε_s) can be obtained from the phase shift, while the unknown dielectric constant, ε_{r2}, can be calculated using the following equation:

$$\varepsilon_{r2} = d_2 \left[\pm \left(\frac{\sum_{i=1}^{3} |d_i|}{\varepsilon_s} - \frac{|d_1| + |d_3|}{|\varepsilon_{r1}|} \right) \right]^{-1}, \tag{19}$$

where coefficients d_i can be determined using Eq. (16).

The example of the calculated unknown dielectric constant in tri-layered configuration is shown in **Figure 7**. The dielectric constants used for this configuration

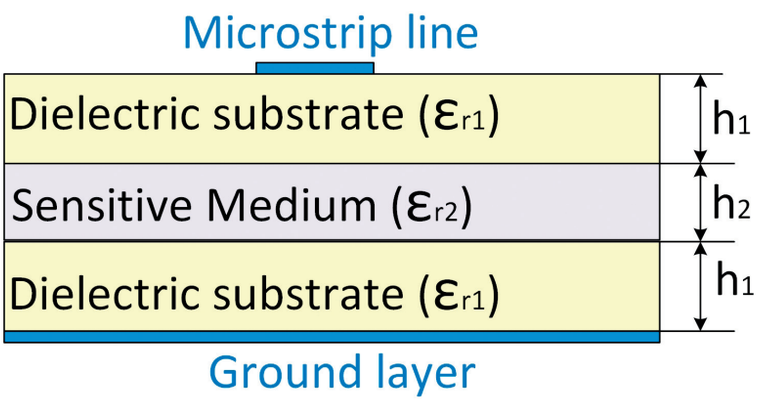

Figure 6.
Microstrip line on tri-layered substrate.

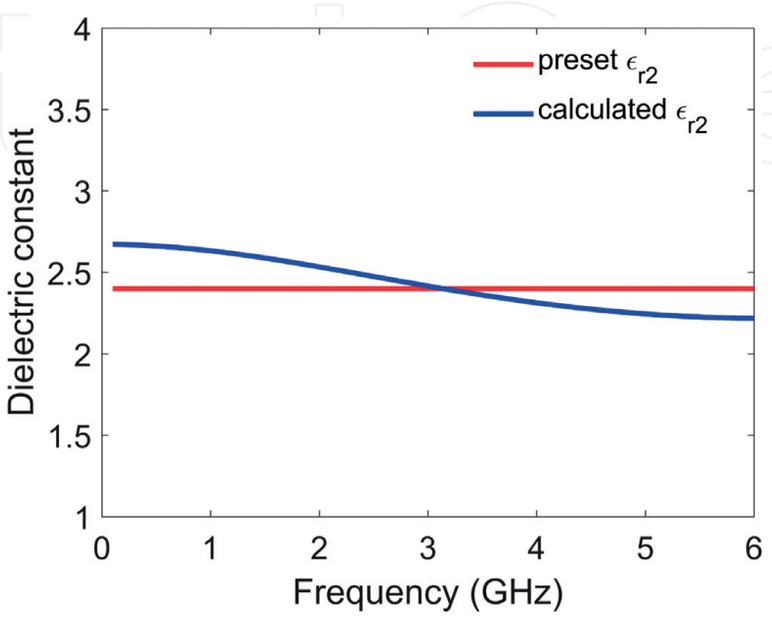

Figure 7.
Calculated unknown dielectric constant in the tri-layered substrate configuration.

were set to constant values of ε_{r1} = 3.6 and ε_{r2} = 2.4, while the geometrical parameters of the microstrip line were set to h_1 = 0.1 mm, h_2 = 0.2 mm, w = 1.5 mm, and L = 10 mm. Good agreement is obtained with the maximal relative error of 10% in the observed frequency range.

The third configuration in which the substrate with an unknown dielectric constant is embedded into the substrate with known properties and dimensions is shown in **Figure 8**. This configuration is particularly interesting for the microfluidic applications, for the characterization of the fluid inside the channel [21].

This configuration of the substrate can be observed as a tri-layered substrate in which the middle layer is composed of two materials with different dielectric constants, ε_{r1} and ε_{r2}. The first and third layers are with known dielectric constant, ε_{r1}. If we assume that all geometrical parameters are known, the calculation of the effective dielectric constants of the middle layer ($\varepsilon_{r1_{eff}}$) can be calculated using Eq. (19). This formula does not determine the unknown dielectric constant, just the effective dielectric constant of the middle layer. Therefore, the unknown dielectric constant ε_{r2} can be calculated using Bruggeman formalism [27]:

$$\varepsilon_{r2e} = V\varepsilon_{r2} + (1 - V)\varepsilon_{r1}, \tag{20}$$

where V is the volumetric fraction of the microfluidic channel in the surrounding substrate. The dielectric constant of the unknown embedded material can be

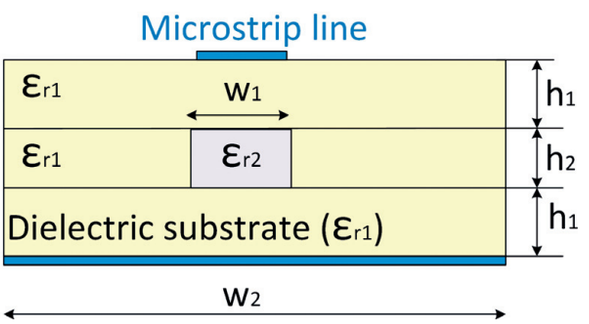

Figure 8.
Microstrip line on the substrate with embedded rectangular channel.

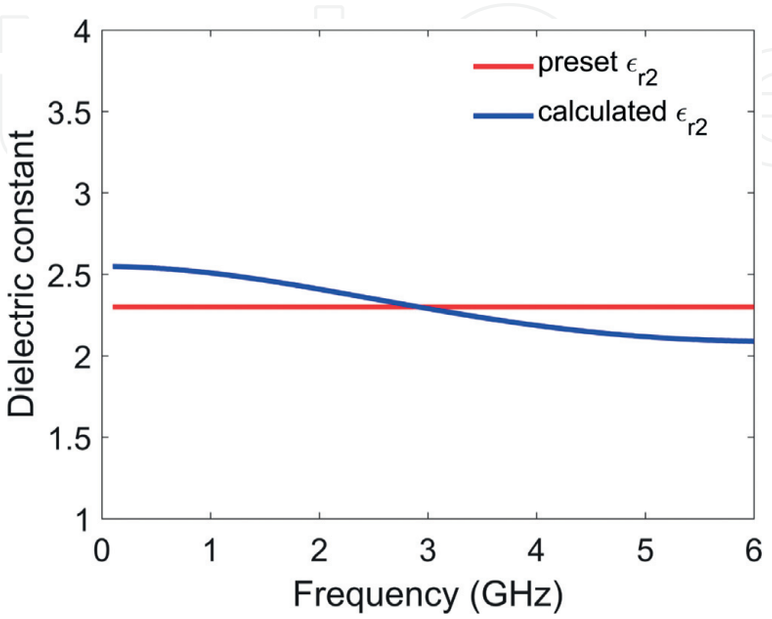

Figure 9.
Calculated unknown dielectric constant in substrate configuration with embedded channel.

determined using the procedure for the extraction of the effective dielectric constant of the tri-layered substrate from the phase shift combined with Eqs. (19) and (20).

The example of the calculated unknown dielectric constant in the embedded substrate configuration is shown in **Figure 9**. The preset values in this case were set to constant values of ε_{r1} = 3.6 and ε_{r2} = 2.35, while the geometrical parameters of the microstrip line were set to h_1 = 0.1 mm, h_2 = 0.2 mm, w = 1.5 mm, and L = 10 mm. The good agreement between the calculated dielectric constant and the preset value is obtained with the relative error lower than 8.5%.

From the previous examples, it can be seen that the phase-shift method has a potential for the characterization of the unknown dielectric materials in different configurations with a good accuracy, and therefore it presents good choice for the rapid characterization of material.

4. Techniques for increasing the phase shift

This section summarized various innovative techniques that can be used for improvement of the sensitivity of phase-shift measurement in the microstrip architecture and their advantages over conventional design.

The first technique is based on increasing the effective length of the transmission line, that is, increasing the inductance and capacitance of the microstrip line. However, this technique results in increased length and reduction in the compactness of the structure. To preserve compactness and satisfy the requirements for good performances, different shapes of the microstrip line have been recently used [28–31]. Since the space-filling property of a fractal offers high potentials for miniaturization of microwave circuits [28–31], the application of the fractal curves theoretically allows the design of infinite-length lines on finite substrate area. In that manner compact transmission line with improved phase response can be obtained using fractal curves. Based on that principle, we have designed a compact soil moisture sensor [28] that consists of two parallel fractal line segments, where each segment comprises two Hilbert fractal curves of the fourth order connected in serial, **Figure 10a**. The additional analyses confirm that the increase of the iteration of the Hilbert fractal curve

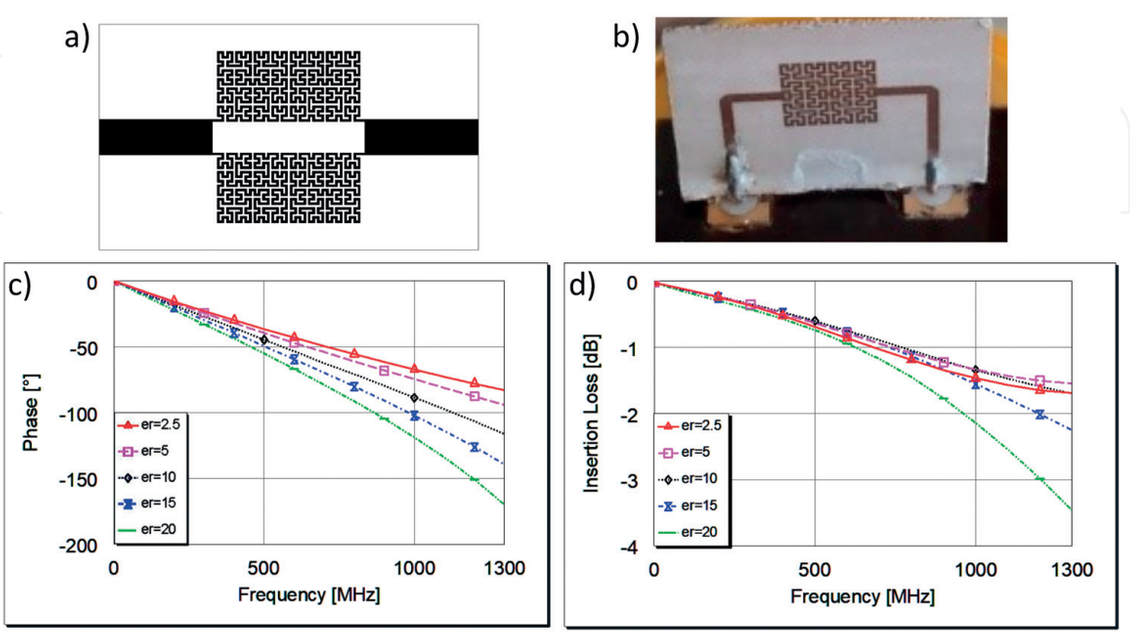

Figure 10.
Soil moisture sensor based on Hilbert fractal curve: (a) layout of the sensor, (b) fabricated sensor, (c) phase-shift response, and (d) insertion loss [28].

increases the range of phase shift [32], but accordingly the insertion loss too. Therefore, in the proposed configuration, two transmission lines are connected in parallel to reduce insertion losses. When Hilbert fractal curves are connected in parallel, the range of the phase shift is approximately the same, but insertion losses are reduced. The Hilbert curve itself is realized with the line width and the spacing between the lines of 100 μm. The results of the proposed sensor placed in the medium with different values of the dielectric constants are shown in **Figure 10**. The range of the phase shift for this configuration at the frequency of 1.2 GHz is 66.64°, while the insertion loss in the worst case is 2.98 dB. The consequence of the line modification is 0.4 dB greater insertion loss comparing to the conventional microstrip line. Although the insertion loss in this case is larger, it is still within acceptable range of 3 dB. However, for the same line length, the range of the phase shift is increased for more than three times. Stated results show that the usage of Hilbert fractal curve leads to more compact sensor characterized by higher sensitivity.

Another technique to increase the phase shift is based on an aperture in the ground plane, where the part of the ground plane, positioned under Hilbert curves of the sensor, shown in **Figure 11**, was removed. In this manner a certain passage for the lines of the electric field is made, so they can pass through it into the soil under the sensor and end up at the bottom side of the ground plane, **Figure 11**. In this manner, soil moisture has larger effect on the sensor characteristics. The results for the sensor with the aperture in the ground plane are presented in **Figure 11**. It can be seen that the range of the phase shift for the sensor with the aperture in the ground plane is 70.76° at the frequency of 1.2 GHz, and the insertion loss is 2.98 dB. Modification in ground plane improved the range of the phase shift for additional 6%, while insertion loss did not change. Quartz sand was used to validate the sensor performances, and the phase-shift measurements were performed for different moisture levels, at operating frequencies in the range of 500–2500 MHz [33, 34]. To investigate the influence of the conductivity, that is, of the soil type, on the calibration curves, the measurement procedure was repeated for the sand moisturized with water with two different salinities (conductivities): 29 and 70‰. If the operating frequency is sufficiently high, Eq. (4) will be satisfied. Therefore, the electrical conductivity can be neglected, and the expression for the phase velocity can be

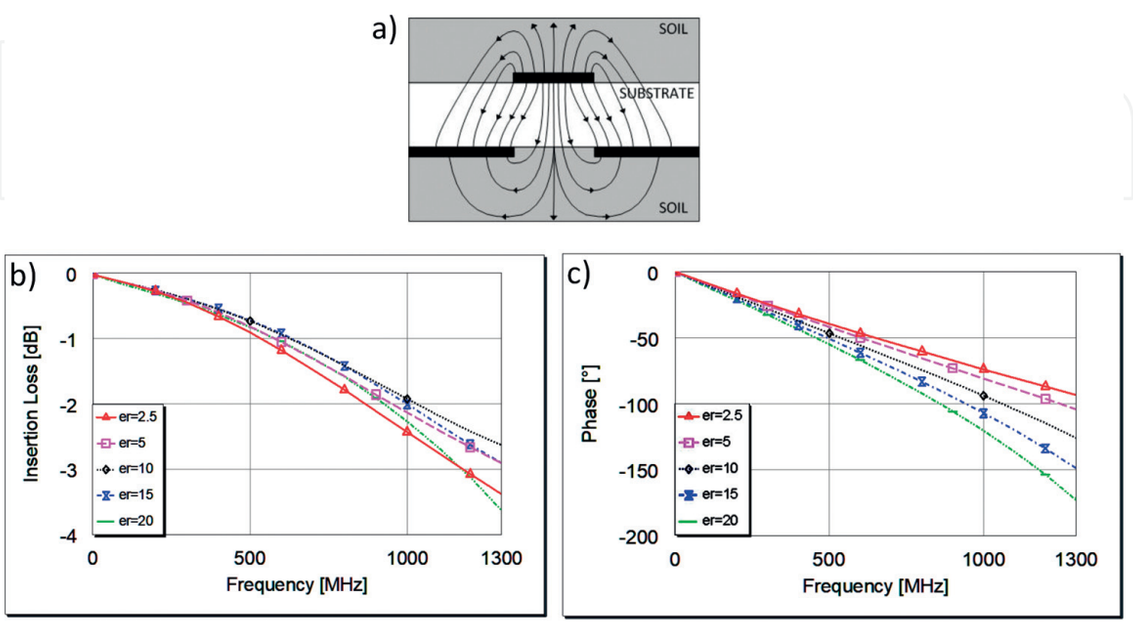

Figure 11.
Soil moisture sensor with the aperture in the ground plane: (a) cross section, (b) phase-shift response, and (c) insertion loss [28].

DOI: http://dx.doi.org/10.5772/intechopen.81790

simplified to Eq. (5). In (**Figure 12**), fitted calibration curves (volumetric water content in the function of the phase shift) for the measurement performed at 500 and 2500 MHz are presented. A significant difference between the calibration curves is obtained at 500 MHz from differently treated samples. However, if the operating frequency is 2500 MHz, the phase shifts obtained from all three samples are almost identical. These results indicate that the Hilbert sensor with the aperture in the ground plane can be successfully used to measure soil moisture independently of the soil type (**Figure 12**).

Third technique to improve sensitivity is based on a defected electromagnetic bandgap (EBG) structure, periodical structure realized as a pattern in the microstrip ground plane. A concept to improve microstrip sensor sensitivity based on the EBG structure was firstly proposed in [35], where it is demonstrated that the sensor sensitivity can be increased by reducing the wave group velocity of the propagating signal. Illustration of this technique is shown in **Figure 13** in the realization of the 3D-printed microfluidic sensor for the determination of the characteristics of different fluids in the microfluidic channel [14]. The bottom layer of the sensor, shown in **Figure 13c**, represents the ground plane realized using defected EBG structure, periodical structure that consists of etched holes. The introduction of the uniform EBG structure in the ground plane forms a frequency region where propagation is forbidden, that is, bandgap in the transmission characteristic [36], while the defect in the EBG results in a resonance in the bandgap, which frequency is determined by the size of the defect. Introduction of the defected EBG structure improves phase shift of the microstrip line in comparison to the conventional microstrip line. Moreover, in comparison with a conventional microstrip line, the intensity of the electric field is stronger in the vicinity of the defect in the EBG [14]. Therefore, the changes of the dielectric constant of the liquid that flows in the channel will have the highest impact to the phase response. In the proposed configuration, the EBG structure is designed to provide bandgap between 5 and 9 GHz, while the defect in the EBG causes the resonance at 6 GHz. By introducing defected EBG structure, the phase change significantly increases, especially at the frequencies that are close to the bandgap edges and at the resonance in the bandgap, due to decrease in the wave phase velocity. From the transmission characteristic, **Figure 14**, it can be seen that the resonant frequency of the defect in the bandgap slightly shifts due to the change of the dielectric constant of the fluid in microchannel. The effect of the EBG structure is predominant at the frequency of 6 GHz where the wave phase velocity is minimal. The results show that the change of the fluid permittivity from 1 (air) to

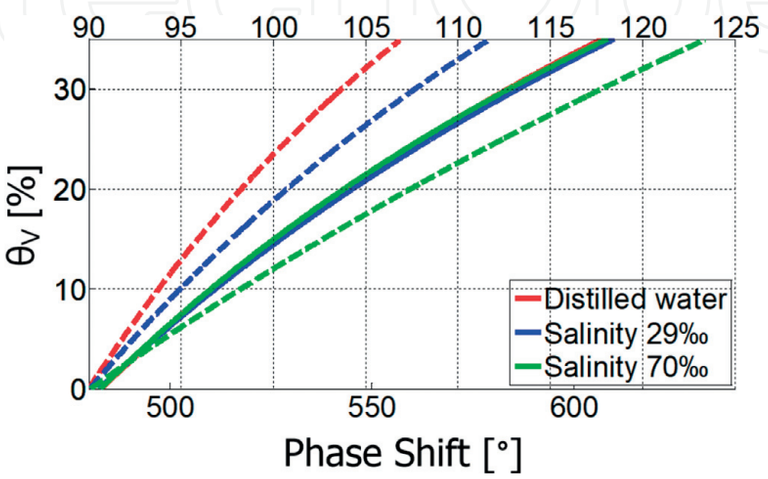

Figure 12.
Volumetric water content for 500 MHz (dashed lines, upper abscissa) and 2500 MHz (full lines, lower abscissa) [33, 34].

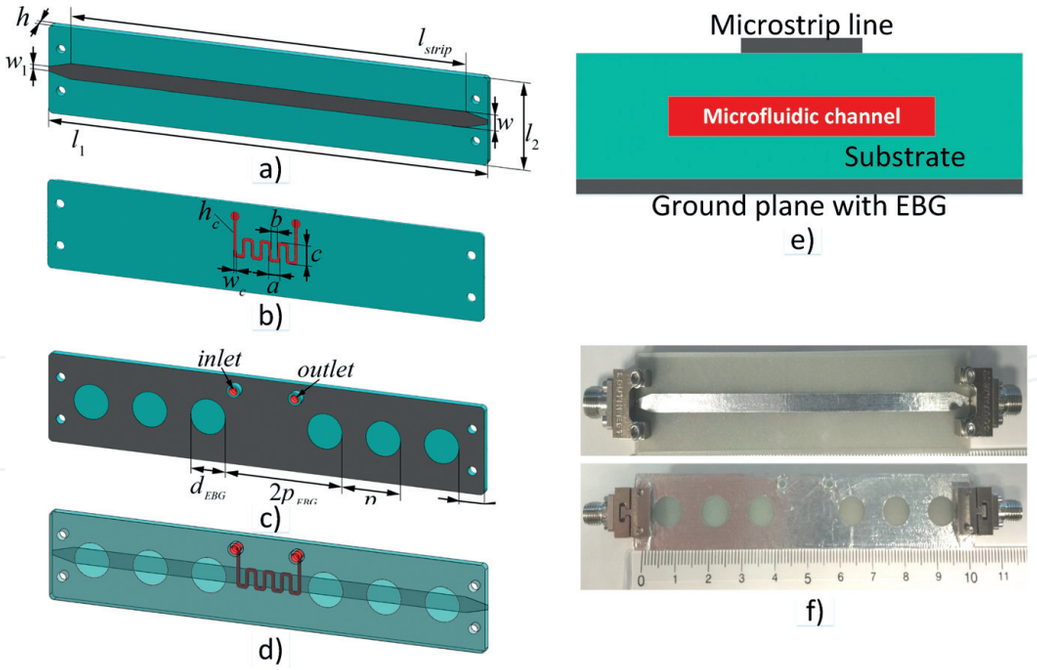

Figure 13.
Microfluidic EBG sensor: (a) top layer, (b) substrate with embedded channel, (c) bottom layer with defected EBG, (d) 3D view, (e) cross section, and (f) top and bottom side of the fabricated sensor [14].

81 (water) causes the phase-shift difference of 84°, **Figure 14**. Compared to the phase shift of the conventional microstrip line without EBG which is only 10.2° at 6 GHz, the proposed design shows eight times higher phase shift. Furthermore, the proposed sensor shows relatively high and almost linear dependence for the fluid materials with permittivity lower than 30. Therefore, the proposed sensor is characterized by relatively high sensitivity and linearity, which makes it a suitable candidate for monitoring small concentrations of a specific fluid in different mixtures. The potential application has been demonstrated in the realization of the microfluidic sensor for detection of toluene concentration in toluene-methanol mixture [14], **Figure 15**.

The fourth technique is based on metamaterials and a left-handed (LH) transmission line approach [37, 38]. Metamaterials are artificial structures that can be designed to exhibit specific electromagnetic properties not commonly found in nature. Metamaterials with simultaneously negative permittivity and

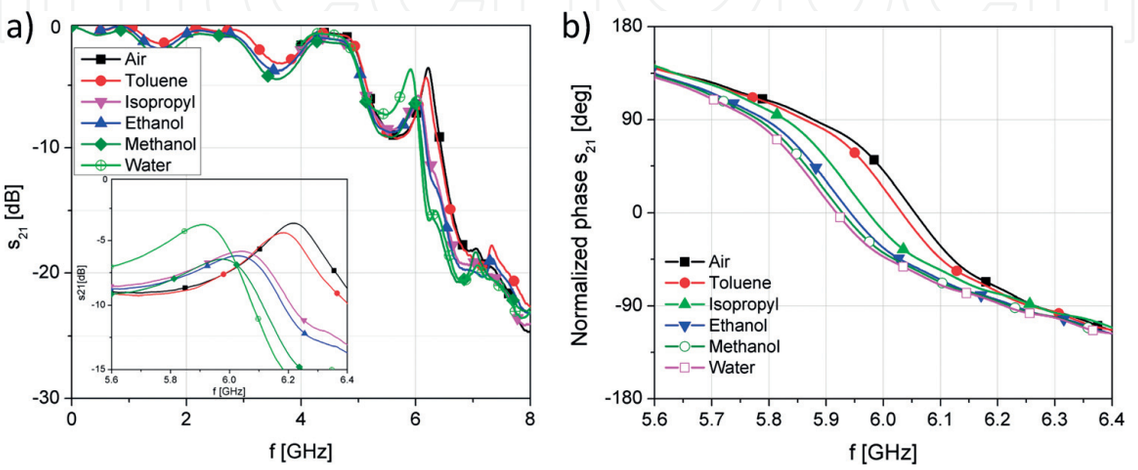

Figure 14.
Measured results of the microfluidic EBG sensor with different fluids inside the microfluidic channel: (a) transmission characteristic and (b) phase characteristic [14].

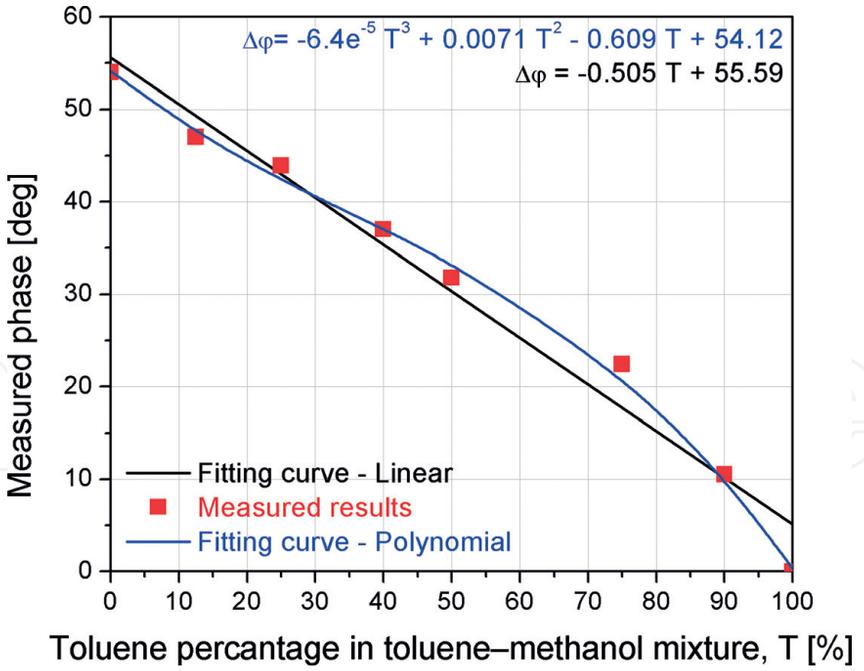

Figure 15.
Measurement of the toluene concentration in toluene-methanol mixture: sensor measured response (dots) and the corresponding fitting curves (lines) [14].

permeability, more commonly referred to as LH materials, have a propagation constant equal to zero at non-zero frequency [37]. Therefore, they can support electromagnetic waves with a group and phase velocities that are antiparallel, known as backward waves [39]. Consequently, energy will travel away from the source, while wave fronts travel backward toward the source. However, the ideal LH structure does not exist in the nature and can be formed as a combination of the LH section and conventional transmission line (RH). This structure known as a composite left-/right-handed (CLRH) transmission line can be formed using a capacitance in series with shunted inductance. In the case of CLRH due to the backward wave propagation, the phase "advance" occurs in the LH frequency range, while phase delay occurs in the RH frequency range [38]. This concept was used in the design of microfluidic sensor for the measurement of the characteristic of the fluid that flows in the microfluidic reservoir placed under CLRH transmission line. The conventional microstrip line in phase comparator was replaced with CRLH transmission line, **Figure 16**. Since the proposed line consists of one CRLH unit cell, it provides passband response at frequency of 1.9 GHz that is characterized with narrowband LH behavior. Therefore, the phase advance at Output 2 is obtained comparing to the signal that propagates true the conventional RH line (Output 1), **Figure 17b**. By changing the properties of the fluid that flows in the microfluidic channel, the central resonance of the LH band slightly shifts to the lower frequency, **Figure 17a**, while the slope of the phase characteristics intensely changes, **Figure 17b**. It can be mentioned that the level between two signals is lower than 8 dB in the worst case at 1.9 GHz; therefore the standard phase detector can be used for the phase-shift measurement. In the proposed configuration, the conventional RH line was used as a referent one, and therefore it was bent in the meander shape to provide maximal measurement phase-shift range at 1.9 GHz. The proposed sensor is characterized with maximal achievable sensitivity, good linearity, and design flexibility, since the maximum extent of the phase can be obtained for the arbitrary range of the dielectric constants by simple modification of the CLRH transmission line.

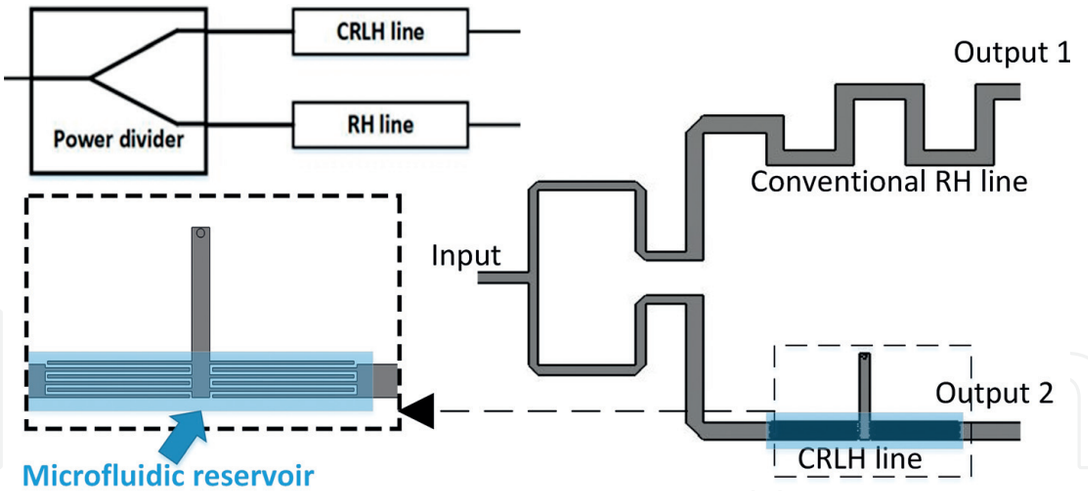

Figure 16.
Blok diagram and layout of the CRLH sensor.

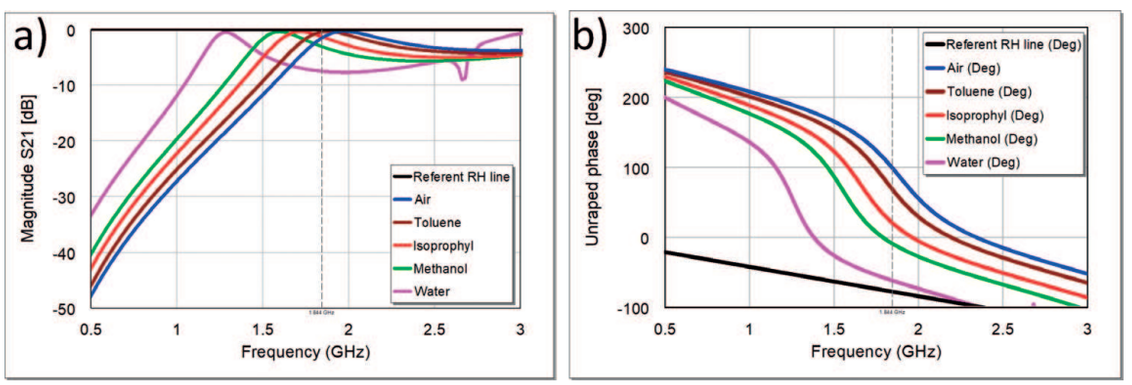

Figure 17.
Response of the CLRH sensor: (a) transmission characteristic and (b) phase characteristic.

5. Simple in-field detection circuit

The phase-shift method, as it was stated above, is the simple method that can be used for the determination of the complex permittivity. Therefore, the expensive instrument for the determination of permittivity can be replaced with a simple detection circuit. The block diagram, and detailed electrical scheme for measurement of the phase shift at single operating frequency, is presented in **Figure 18** together with the fabricated prototype realized in LTCC (low-temperature cofired ceramics) technology.

Detection circuit consists of a microwave oscillator, a quadrature hybrid, a sensor element, and a phase detector functional blocks. The operating principle can be described in the following way: sinusoidal signal generated by source, that is, microwave oscillator, is divided by quadrature hybrid on measurement and referent signal. The measurement signal propagates along sensor element where phase shift occurs according to the dielectric properties of the surrounding medium. The signal from the sensor element is fed into the input of the phase detector which compares the phase of the measurement and the referent signal. The output of the phase detector is the voltage proportional to the phase shift of the input signals which can be related to the measured dielectric constant. Referent signal propagates through the phase-shifter module which has a purpose to provide the calibration of the sensor and to overcome deviations of the nominal properties of the materials and

DOI: http://dx.doi.org/10.5772/intechopen.81790

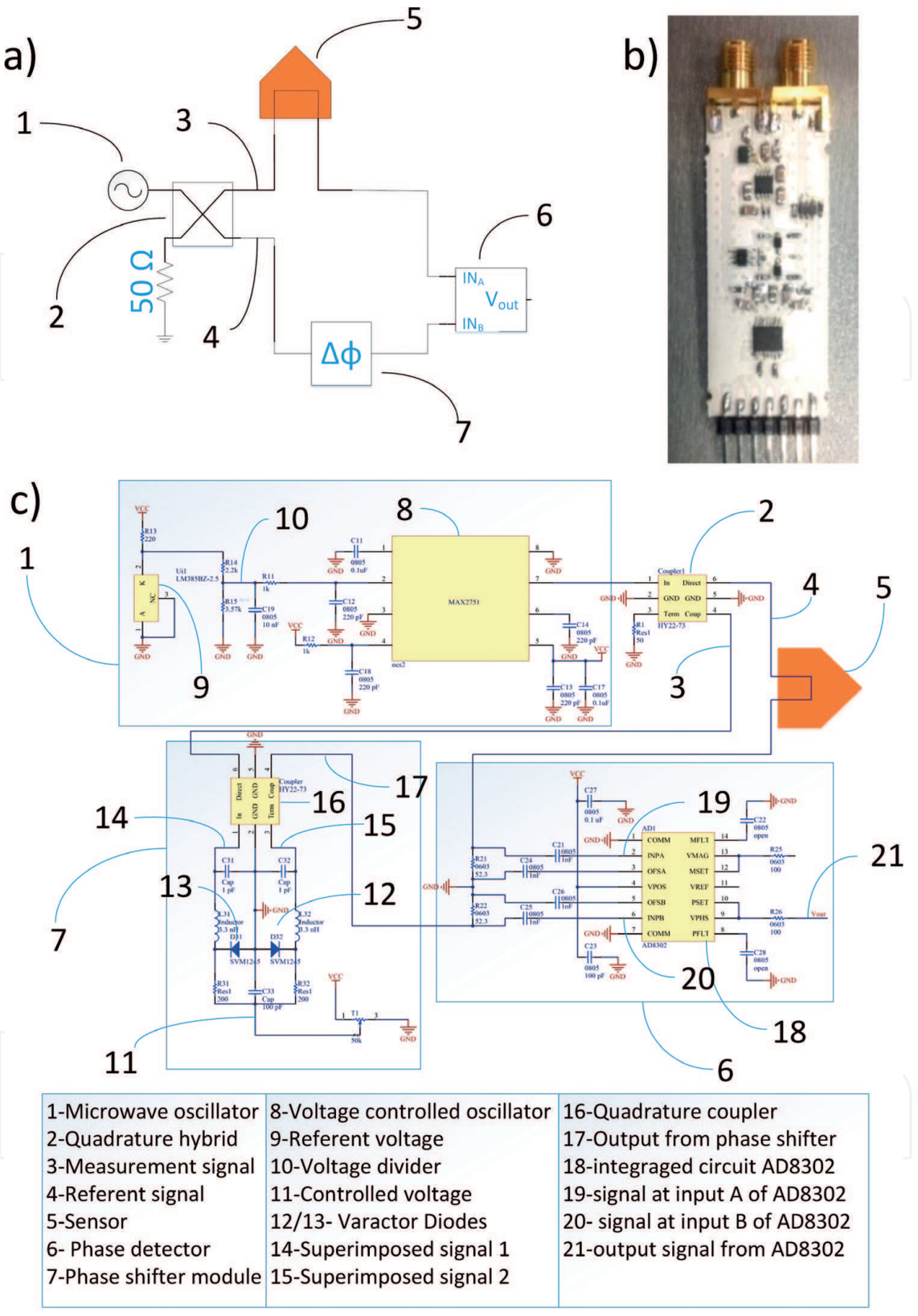

1-Microwave oscillator	8-Voltage controlled oscillator	16-Quadrature coupler
2-Quadrature hybrid	9-Referent voltage	17-Output from phase shifter
3-Measurement signal	10-Voltage divider	18-integraged circuit AD8302
4-Referent signal	11-Controlled voltage	19-signal at input A of AD8302
5-Sensor	12/13- Varactor Diodes	20- signal at input B of AD8302
6- Phase detector	14-Superimposed signal 1	21-output signal from AD8302
7-Phase shifter module	15-Superimposed signal 2	

Figure 18.
Phase-shift measurement device: (a) block diagram, (b) fabricated circuit, and (c) detail electronic circuit of the phase-shift measurement device [13].

components used for sensor fabrication. In this way the repeatability of measurement of the different sensors will be secured.

The phase-shift measurement electrical circuit is detailly presented in **Figure 18c**, indicating abovementioned functional blocks of the circuit, **Figure 18a**. The oscillator is realized by the voltage-controlled oscillator MAX2751 (8), which is

adjusted by the referent voltage (9) and the voltage divider (10) to operating frequency of 2.2 GHz. The signal from the oscillator is divided into measurement and referent signals using commercially available quadrature coupler circuit HY22-73 (2). The phase-shifter module allows control of the phase shift and enables fine-tuning of the difference in the phase between the measurement and referent signals. The phase shift can be achieved by varying the control voltage (11) that affects the capacitance of the varactor diodes (12 and 13). The change in capacitance affects the signals (14) and (15) which superimpose with the input referent signal (3) through the quadrature coupler (16) and in this way changes the phase of the resultant signal at the output of the module (17). The measurement of the phase shift between the measurement and referent signal is done using a phase detector module implemented with the integrated circuit AD8302 Analogue Devices (18). The phase detector circuit is set to the phase difference measurement mode according to the manufacturer's recommendation. Integrated circuit AD8302 on its output (21) gives a voltage signal that is proportional to the phase difference of the signal on its inputs (19) and (20).

The accuracy of the designed phase-shift measurement device was experimentally verified by comparing the results of the measurement of the phase shift of the signal, induced by phase-shift circuit (functional block (7), **Figure 18c**), in the range from 0 to 90° with the results of the measurement obtained using vector network analyzer (VNA). The results of the comparison are shown in **Figure 19**. It can be seen that the results agree well and the relative error in respect of the full-scale output is 5.56% which confirms performance of the designed phase-shift circuit.

Additional module for different sensor topologies can be designed to provide a conversion of the measured voltage to the corresponding value of the dielectric constant.

6. Conclusions

In this chapter dielectric characterization technique based on the phase-shift method has been presented. It has been shown that both the real and imaginary part of a complex permittivity can be calculated solely by using the phase shift of the transmitted signal. The exact formulas for the calculation of the unknown dielectric properties in the microstrip and multilayered substrate configurations such as bilayered, tri-layered, and embedded configurations were presented.

To enhance sensitivity of sensors that operate on phase-shift principle, various techniques for increasing the phase-shift range have been presented. The first technique uses space-filling property of Hilbert fractal curve to increase the phase-shift range and yet preserve the compactness of the structure. The technique that increases sensitivity of the sensor by introducing an aperture in the ground layer has been presented on the example of the soil moisture sensor. The third technique based on EBG effect has been illustrated on the example of 3D-printed microfluidic sensor for detection of toluene concentration in toluene-methanol mixture. Metamaterial and CRLH transmission line approach is used as the technique in the realization of microfluidic sensor with a maximum extent of the phase-shift range.

In the end a simple in-field detection circuit for determination of permittivity based on the phase-shift measurement on single operating frequency has been described. With the help of described concepts, a complete set of tools has been introduced which enables the design and optimization of the phase-shift-based sensors.

DOI: http://dx.doi.org/10.5772/intechopen.81790

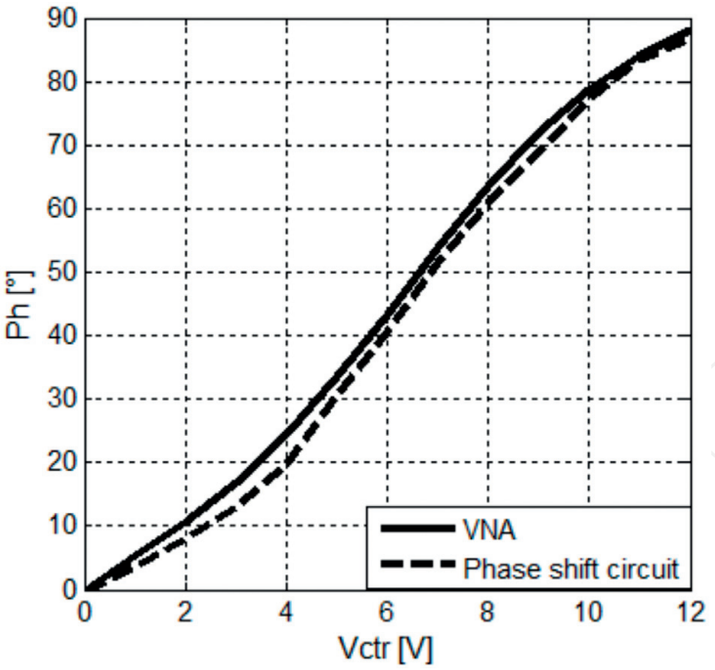

Figure 19.
Comparisons between VNA and designed phase-shift measurement circuit.

Acknowledgements

This result is part of a project that has received funding from the European Union's Horizon 2020 research and innovation programme under the grant agreement No. 664387.

Author details

Vasa Radonic*, Norbert Cselyuszka, Vesna Crnojevic-Bengin and Goran Kitic
University of Novi Sad, BioSense Institute–Research and Development Institute for Information Technologies in Biosystems, Novi Sad, Serbia

*Address all correspondence to: vasarad@uns.ac.rs

References

[1] Foster KR, Schwan HP. Dielectric properties of tissues and biological materials: A critical review. Critical Reviews in Biomedical Engineering. 1989, 1989;**17**(1):25-104

[2] Nelson SO. Fundamentals of dielectric properties measurements and agricultural applications. Journal of Microwave Power and Electromagnetic Energy. 2010;**44**(2): 98-113. DOI: 10.1080/08327823.2010.11689778

[3] Jarvis JB, Janezic MD, Riddle BF, Johnk RT, Kabos P, Holloway CL, et al. Measuring the Permittivity and Permeability of Lossy Materials: Solids, Liquids, Metals, Building Materials, and Negative-Index Materials. NIST Technical Note 1536; 2005

[4] Krraoui H, Mejri F, Aguili T. Dielectric constant measurement of materials by a microwave technique: Application to the characterization of vegetation leaves. Journal of Electromagnetic Waves and Applications. 2016;**30**(12):1643-1660. DOI: 10.1080/09205071.2016.1208592

[5] Brodie G, Jacob MV, Farrell P. Techniques for measuring dielectric properties. In: Microwave and Radio-Frequency Technologies in Agriculture. 1st ed. Warsaw, Poland: Sciendo; 2015. pp. 52-77. DOI: 10.1515/9783110455403-007

[6] Nozaki R, Bose TK. Broadband complex permittivity measurements by time-domain spectroscopy. IEEE Transactions on Instrumentation and Measurement. 1990;**39**(6):945-951. DOI: 10.1109/19.65803

[7] Cataldo A, Tarricone L, Attivissimo F, Trotta A. A TDR method for real-time monitoring of liquids. IEEE Transactions on Instrumentation and Measurement. 2007;**56**(5):1616-1625. DOI: 10.1109/TIM.2007.903596

[8] Keysight Technologies. Basics of Measuring the Dielectric Properties of Materials, Application note, Literature number 5989-2589EN, 2017

[9] Stuchly MA, Stuchly SS. Coaxial line reflection methods for measuring dielectric properties of biological substances at radio and microwave frequencies—A review. IEEE Transaction of Instrumentation and Measurement. 1980;**M-29**:176-183. DOI: 10.1109/TIM.1980.4314902

[10] Chen L, Varadan VV, Ong CK, Neo CP. Microwave Electronics: Measurement and Materials Characterization. 1st ed. Chichester, England: John Wiley & Sons; 2005. DOI: 10.1002/0470020466

[11] Rode & Swartz. Measurement of Dielectric Material Properties. Application Note. RAC-0607-0019, 2012

[12] You KY. Effects of sample thickness for dielectric measurements using transmission phase-shift method. International Journal of Advances in Microwave Technology. 2016;**1**(3): 64-67

[13] Kitic G. Microwave soil moisture sensor based on phase shift method independent of electrical conductivity of the soil. The Intellectual Property Office Republic of Serbia; 2018. П-2018/0253—March 2018

[14] Radonic V, Birgermajer S, Kitic G. Microfluidic EBG sensor based on phase-shift method realized using 3D Printing technology. Sensors. 2017; **17**(4):892. DOI: 10.3390/s17040892

[15] Balanis CA. Advanced Engineering Electromagnetics. New York: John Wiley & Sons, Publisher Inc; 1989

[16] Liu R, Zhang Z, Zhong R, Chen X, Li J. Nanotechnology synthesis study: Technical Report 0-5239-1; April 2007. pp. 76-79

[17] Pozar DM. Microwave Engineering. 4th ed. New Jersey: John Wiley and Sons; 2011

[18] Kuzuoglu M, Mittra R. Frequency dependence of the constitutive parameters of causal perfectly matched anisotropic absorbers. IEEE Microwave and Guided Wave Letters. 1996;**6**(12): 447-449. DOI: 10.1109/75.544545

[19] Steeman PAM, Turnhout JV. A numerical Kramers-Kronig transform for the calculation of dielectric relaxation losses free from Ohmic conduction losses. Colloid and Polymer Science. 1997;**275**(2):106-115. DOI: 10.1007/s003960050059

[20] Lucarini V, Saarinen JJ, Peiponen K-E, Vartiainen EM. Kramers–Kronig Relations in Optical Materials Research. Berlin/Heidelberg: Springer-Verlag; 2005. DOI: 10.1007/b138913

[21] Landau LD, Lifshitz EM. Electrodynamics of Continuous Media. Moscow, Russia: Pergamon Press; 1960

[22] Arfken GB, Weber HJ. Mathematical Methods for Physicists. 6th ed. Burlington, MA, USA: Elsevier Academic Press; 2005, 2005. DOI: 10.1016/C2009-0-30629-7

[23] Jha KR, Singh G. Terahertz Planar Antennas for Next Generation Communication. Cham, Switzerland: Springer International Publishing; 2014. DOI: 10.1007/978-3-319-02341-0

[24] Whittaker ET, Watson GN. A Course in Modern Analysis. 4th ed. Cambridge, England: Cambridge University Press; 1990. DOI: 10.1017/CBO9780511608759

[25] Lee K, Hassan A, Lee CH, Bae J. Microstrip patch sensor for salinity determination. Sensors. 2017;**17**(12): 2941. DOI: 10.3390/s17122941

[26] Jankovic N, Radonic V. A microwave microfluidic sensor based on a dual-mode resonator for dual-sensing applications. Sensors. 2017;**17**(12):2713. DOI: 10.3390/s17122713

[27] Lakhtakia A, Michel B, Weiglhofer WS. Bruggeman formalism for two models of uniaxial composite media; dielectric properties. Composites Science and Technology. 1997;**57**: 185-196. DOI: S0266353896001224

[28] Radonic V, Kitic G, Crnojevic-Bengin V. Novel Hilbert soil moisture sensor bassed on the phase shift method, In: Proceedings of Mediterranean Microwave Symposium (MMS 2010); 25–27 August 2010; Guzelyurt, Cyprus; 2010

[29] Crnojevic-Bengin V, Radonic V, Jokanovic B. Fractal geometries of split-ring resonators. IEEE Transactions of Microwave Theory and Techniques. 2008;**56**(10):2312-2321. DOI: 10.1109/TMTT.2008.2003522

[30] Jarry P, Beneat J. Design and Realizations of Miniaturized Fractal Microwave and RF Filters. 1st ed. Hoboken, NJ, USA: Wiley; 2009. ISBN: 978-0-470-48781-5

[31] Stojanović G, Radovanović M, Radonic V. A New Fractal-Based Design of Stacked Integrated Transformers, Active and Passive Electronic Components; 2008. Article ID 134805. DOI: 10.1155/2008/134805

[32] Kitic G. Microwave soil moisture sensors based on distributed elements [thesis]. University of Novi Sad, Faculty of Technical Sciences; 2015

[33] Will B, Crnojević-Bengin V, Kitić G. Microwave soil moisture sensors. In: Proceedings of the 43rd European Microwave Conference (EuMA); 6–10 October 2013; Nuremberg, Germany. IEEE; 2013. DOI: 10.23919/EuMC.2013.6686793

[34] Kitić G, Crnojević Bengin V. The influence of conductivity on the microstrip soil moisture sensor. In: 3rd Global Workshop on Proximal Soil Sensing; 26–29 May 2013; Potsdam, Germany

[35] García-Baños B, Cuesta-Soto F, Griol A, Catalá-Civera JM, Pitarch J. Enhancement of sensitivity of microwave planar sensors with EBG structures. IEEE Sensors Journal. 2006; **6**:1518-1522. DOI: 10.1109/JSEN.2006.884506

[36] Griol A, Mira D, Martinez A, Marti J. Multiple frequency photonic bandgap microstrip structures based on defects insertion. Microwave and Optical Technology Letters. 2003;**36**:479-481. DOI: 10.1002/mop.10795

[37] Christophe Caloz C, Itoh T. Electromagnetic Metamaterials: Transmission Line Theory and Microwave Applications. 1st ed. Wiley-IEEE Press; 2005. DOI: 10.1002/0471754323

[38] Lai A, Itoh T, Caloz C. Composite right/left-handed transmission line metamaterials. IEEE Microwave Magazine. 2004;**5**(3):34-50. DOI: 10.1109/MMW.2004.1337766

[39] Ramo S, Whinnery JR, Duzer TV. Fields and Waves in Communication Electronics. 2nd ed. New York, NY, USA: Wiley; 1984